Model-Based Cancellation of Biodynamic Feedthrough Using a Force-Reflecting Joystick

R. Brent Gillespie and Szabolcs Sövényi

Abstract— **Manual control performance on-board a moving vehicle is often impeded by *biodynamic feedthrough*—the effects of vehicle motion feeding through the operator's body to produce unintended forces on the control interface. In this paper, we propose and experimentally test a model-based controller that acts through a motorized manual interface to cancel the effects of biodynamic feedthrough. The cancellation controller is based on characterization data collected using an accelerometer on the vehicle and a force sensor embedded in the manual interface and a protocol under which the manual interface is temporarily immobilized while in the grip of the operator. The biodynamic model fit to the data is based in turn on a carefully constructed model of the coupled vehicle-operator system. The impact of biodynamic feedthrough and the ability of the model-based controller to cancel its effects were estimated through an experiment in which 12 human subjects used a joystick to carry out a pursuit tracking task on-board a single-axis motion platform. Cancellation controllers derived from biodynamic models fit individually to each subject significantly improved pursuit tracking performance, as evidenced by a 27% reduction in root-mean-square tracking error, a 35% improvement in time-on-target, and an increase in crossover frequency from 0.1 to 0.14 Hz.**

Index Terms— **biodynamic feedthrough, crossover model, manual control of vehicles, haptic interface.**

I. Introduction

THE performance achievable by a human operator using a manual interface to track a moving target has been studied extensively, especially in aviation applications [1] [2]. The limits of performance of human tracking are influenced by various factors, including the kinematics of the interface device, its mechanical response, features of the associated visual display, and of course the dynamics of the plant under control. A further limiting factor arises if the tracking task is performed on-board a moving vehicle, due to the phenomenon termed *biodynamic feedthrough* or *vibration feedthrough* [3]. By means of biodynamic feedthrough, motions of the vehicle couple through the operator's body and accelerations induce inertia forces that act on the joystick, giving rise to tracking commands quite outside the intentions of the human operator.

The systems in which biodynamic feedthrough plays a role can be divided into two classes according to whether or not the vehicle itself is being controlled through the manual interface. For the case in which the interface is used to control the vehicle, a feedback loop is closed through the operator's body. Acting through the body, vehicle motion produces motion of the manual interface, which in turn produces further vehicle motion. As a result, oscillations may appear in the human-machine system—oscillations that will grow or become unstable with sufficient loop gain and accumulated phase difference. Because these oscillations can jeopardize safe operation of the vehicle, they have attracted significant attention in the literature. Oscillations appearing in the roll behavior of joystick-controlled high-performance aircraft were analyzed in [4] and [5]. Biodynamic feedthrough also appears in the drive dynamics of powered wheelchairs and hydraulic excavators [6], [7]. Biodynamic feedthrough might also play a role in inciting or exacerbating another feedback loop whose stability is occasionally compromised, namely Pilot Induced Oscillations (PIO). PIO arise due to time delays in human perception and cognition in the volitional control loop, whereas feedthrough oscillations involve only biomechanical and vehicle response. Yet the gain or phase margins associated with the volitional loop can be exceeded, giving rise to PIO, when the volitional loop is coupled with or disturbed by feedthrough dynamics [8].

The second class of system in which biodynamic feedthrough plays a role does not feature a feedback loop through the operator's body. In these systems the object being moved or steered through the interface is a machine or object other than the vehicle—an auxiliary controlled element. In this case, biodynamic feedthrough may be interpreted as a path by which a disturbance enters the volitional control loop. As vehicle passengers take on an increasing number of manual control tasks while on-board ground and air vehicles, the role of biodynamic feedthrough in auxiliary system control becomes more and more relevant. Especially in modern military operations, manual control input is required of crew-members while underway. Examples include remote-control of unmanned vehicles from on-board a moving command vehicle. The design of interface to informatics devices in commercial trucks and automobiles also requires attention to the effects of biodynamic feedthrough.

Various approaches have been proposed to mitigate the effects of biodynamic feedthrough. Perhaps the most straightforward and often effective means is to redesign the kinematics of the interface or configure an arm or handrest to stabilize the hand. A steering wheel, for example, is essentially immune to translational accelerations whereas a joystick is quite sensitive because of the largely translational displacements of the hand gripping the joystick. Another countermeasure involves modifying the mechanical response of the interface device, such as increasing joystick damping and/or stiffness [6]. Also, so-called *motion sticks* are considered more immune to biodynamic feedthrough than *force sticks* (also called *stiff*

Manuscript revised September 23, 2005

Both authors are with the Department of Mechanical Engineering, University of Michigan .

sticks) [3]. Short of interface re-design, signals within the system comprising the vehicle, human, and controlled element (whether or not the controlled element is the vehicle) can be manipulated to mitigate biodynamic feedthrough. Gains can be reduced [6] or reduced selectively according to frequency content using a filter. Some of these approaches, however, also compromise human-in-the-loop or tracking control performance. Alternatively, a filter can be used to remove only the portion of the command signal due to biodynamic feedthrough, when that filter is designed according to a model of biodynamic feedthrough. Grunwald et al. [9] demonstrated the utility of such a filter and Verger et al. extended the approach to an adaptive filter [10].

The use of a motorized control interface for cancellation of biodynamic feedthrough was proposed in [11] and [12] and further developed in [13] and [14]. In this approach, an estimate of the biodynamic feedthrough force acting on the joystick is generated using a measure of vehicle motion and a model of the biodynamic system transfer function. That estimate is then applied directly to the interface through the action of a motor. Ideally the interface itself, as the site at which the forces cancel, should respond as if biodynamic feedthrough were not present. As a result, the interface has a different mechanical feel to it. Sirouspour and Salcudean [13] [14] describe the use of a controller whose design is optimized to simultaneously cancel feedthrough effects and match a desired interface admittance. Their investigation covered only the vehicle control case and used a model of biodynamic feedthrough based only on the driving point impedance of the operator. Also, Repperger [8] has investigated the use of a motorized joystick (a haptic interface) for mitigating PIO.

In this paper we address the second class of systems, in which the controlled element is not the vehicle. We first develop a model of biodynamic feedthrough in section II and based on that model, we design a system identification experiment that allows us to fit a model for the human transmittance. The transmittance model is then used as a cancellation controller that injects its effort through a motor coupled to the interface device, as described in section III. We investigate the utility of our compensation controller in the context of a pursuit tracking task, and use the well-known crossover model by McRuer [2] to analyze human performance with and without the controller in place. We also incorporate trials without vehicle motion into our experiment to establish baseline tracking performance for each subject. Results from a human subject experiment are presented in section IV.

II. Modeling the Human-Vehicle System

In this section we develop a model of the interacting human operator and vehicle—a model aimed specifically at capturing the effects of vehicle motion on manual control performance. Naturally, the most interesting part of the system model pertains to the human operator. Our model for the operator has two main sub-models: The first is a description of the mechanics of the operator's body that is responsible for transmitting mechanical energy between the vehicle seat and the manual control interface. This sub-model, which we call the biodynamic model, does not include any volitional control. The second component of the operator model describes volitional response to visual input pertaining to a pursuit tracking task. We call this sub-model the volitional tracking model.

To begin the development of the system model, let us briefly introduce our experimental apparatus (Figure 1) as a representative ground vehicle (a more complete description will be given in section III below). The apparatus is a single-axis motion platform capable of simulating the lateral motions of a ground vehicle while an operator attempts to perform a manual control task on-board that vehicle. The operator is seated in a chair on the platform and uses his right hand to grasp a joystick also mounted on the platform. Through the joystick, and using visual feedback, the operator may cause a cursor on a computer screen to follow a target that moves in an unpredictable fashion. The target following task is modeled after the well-known pursuit tracking task and is representative of a large family of manual control tasks that might be undertaken on-board a vehicle.

Our apparatus produces motion in the lateral direction only, for which we draw justification from the observation that biodynamic feedthrough, when it appears in a real-world vehicle, produces motion predominantly in a particular axis and does not seem to depend on coupling between axes. Although the apparatus has limited workspace, it can nevertheless be used to induce biodynamic feedthrough since the phenomenon usually involves only small to moderate amplitude vehicle oscillations.

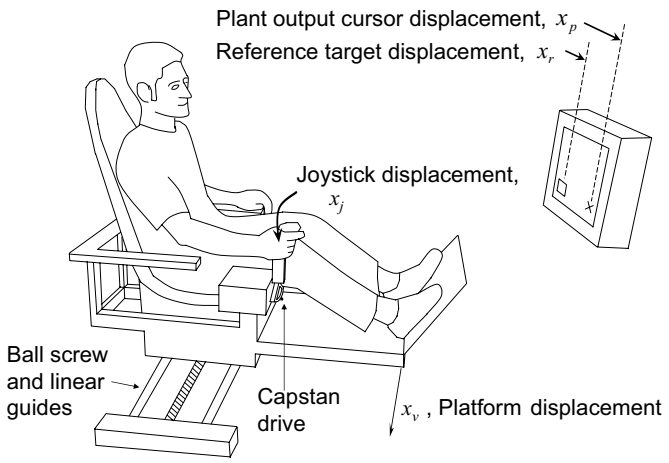

Fig. 1. A human operator seated on a single-axis motion platform uses a joystick to cause a cursor on the screen to track a target that moves in an unpredictable fashion. The translational axis of the motion platform is perpendicular to the rotational axis of the joystick; thus both the platform and hand motions are in the lateral direction.

We begin our model development by noting the two mechanical interfaces that exist between the operator's body and the environment. The first mechanical interface lies between the seat and operator's trunk and the second lies between the joystick and the operator's hand. For each mechanical interface, a force and a velocity may be defined to characterize the interaction. Let the interaction force f_s and common seat/trunk velocity $\dot{x}_v$ characterize mechanical interactions between the seat and trunk of the operator and let the interaction force

f_b and the hand/joystick contact velocity $\dot{x}_j$ characterize the hand/joystick interactions. Between these four variables, there exist four transfer functions. Two driving-point impedances, denoted Z_{11} and Z_{22}, describe how vehicle velocity $\dot{x}_v$ and joystick velocity $\dot{x}_j$ impact vehicle force f_s and joystick force f_b, respectively. The other two transfer functions are transmittances Z_{12} and Z_{21} that describe how vehicle velocity $\dot{x}_v$ and joystick velocity $\dot{x}_j$ affect joystick force f_b and vehicle force f_s, respectively. The four transfer functions are assembled into a two-port shown inside the dashed box in Figure 2. Note that although the joystick rotates about a horizontal axis, we define the displacement x_j of the hand as a translational displacement, measured relative to the platform, since the angular workspace is small (30°) and the distance from pivot to hand is large (10 cm). The path from $\dot{x}_v$ through the block $s\ m_j$ accounts for the effect of vehicle acceleration on the mass of the joystick. Assuming small joystick displacements x_j, the equivalent mass m_j accounts for the inertia force that acts on the joystick due to the acceleration $\ddot{x}_v$ of the moving vehicle.

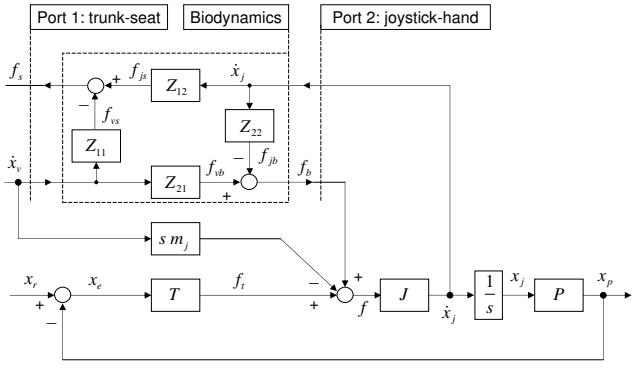

Fig. 2. The human operator is modelled as a two-input, two-output system in which the input velocity $\dot{x}_v$ and output force f_s comprising port 1 capture the interaction between the trunk and the vehicle seat, while the output force f_b and input velocity $\dot{x}_j$ comprising port 2 describe the interaction between the hand and the joystick. The four impedances capture the input-output maps of the two-port. The transfer function T describes how the operator responds to the visually observed difference between the reference signal x_r and the plant output x_p by imposing a force f_t on the joystick J. The force f_b enters the tracking loop as a disturbance and models the biodynamic response of the human operator to the joystick angular velocity $\dot{x}_j$ and the vehicle velocity $\dot{x}_v$.

A. Modeling the biodynamic system

To highlight the role of biodynamic feedthrough as a disturbance to the tracking loop, the block diagram in Figure 2 may be re-arranged and simplified to arrive at the block diagram in Figure 3. Since the vehicle mass is significantly larger than the mass of the operator, we modeled the vehicle as an ideal motion source and removed the transfer functions Z_{11} and Z_{12}. The two pathways from vehicle velocity $\dot{x}_v$ through Z_{21} and sm_j were combined by defining $f_b' \equiv f_b + sm_j\dot{x}_v$ and by defining $H \equiv Z_{21}/s - m_j$ to create the single pathway from vehicle acceleration $\ddot{x}_v$ through the transfer function H shown in Figure 3. Note that the input to H is now the vehicle acceleration $\ddot{x}_v$. A block diagram manipulation was used to move the driving point impedance Z_{22} to its position in feedback around the joystick J. The role of the vehicle acceleration $\ddot{x}_v$ acting through the biodynamic model H is now apparent as a disturbance acting on the tracking control loop.

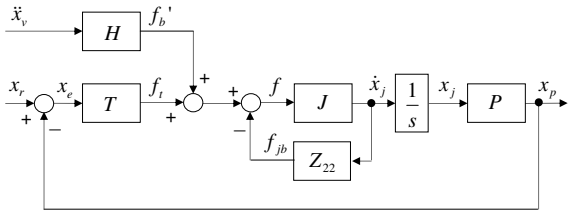

Fig. 3. In this block diagram, biodynamic feedthrough can be recognized as a pathway by which vehicle acceleration $\ddot{x}_v$ enters the tracking loop as a disturbance. This block diagram follows from that in Figure 2 after removing Z_{12} and Z_{11} under the assumption that the vehicle acts as a motion source and after defining $H \equiv Z_{21}/s - m_j$ and moving Z_{22} into position as a feedback loop around the joystick J.

We propose to mitigate the effects of biodynamic feedthrough on tracking by injecting an estimate $\hat{f}_b'$ of the force f_b' into the tracking loop. We will inject $\hat{f}_b'$ through the action of a motor coupled to the joystick such that its direction opposes that of f_b'. In Figure 1, the capstan drive that couples a DC motor inside the joystick box to the joystick is noted. To produce the estimate $\hat{f}_b'$, we assume that a measure of vehicle acceleration $\ddot{x}_v$ is available (perhaps through an accelerometer). Thus $\hat{f}_b'$ will be constructed using an estimate $\hat{H}$ of the biodynamic feedthrough function H.

B. Modeling volitional tracking

In contrast to the biodynamic model, a model of an operator whose hand on the joystick responds to visual input to cause a cursor to track a moving target cannot rely strictly on biomechanics. Cognitive processes, in particular visual perception and volitional muscle action are at play in the transfer function T (the controller in the tracking loop) in Figure 3. High-level cognitive processes such as feedforward control or path planning are neglected, since the target moves in an unpredictable fashion, has no preview, and must therefore be continually monitored. If there exists a transfer function in the plant (for example an integrator from steering angle to vehicle heading, as in the simplest model of driving) then the operator must take such behavior into account. Pursuit tracking has been studied extensively and is richly reported in the literature [2]. We have adopted the pursuit tracking task precisely because such models exist, based on experimental observation of human behavior. The most well-known of these models is the "crossover model", first introduced by McRuer [2].

McRuer's crossover model describes the human controller not as an isolated input-output system, but as a member of the open-loop transfer function. The open-loop transfer function, under unity gain feedback as in Figure 3, is the cascade of the controller T, the joystick dynamics, and the plant dynamics P. Let us denote the feedback interconnection of J and Z_{22} together with the integrator as J^*. Then the crossover model

states that the open-loop transfer function TJ^*P has the frequency response, in the region of crossover, of an integrator with a certain time delay. The crossover frequency ω_c is that frequency for which the response has unity gain. In symbols,

$$TJ^*P(j\omega) = \frac{\omega_c e^{-j\omega T_d}}{j\omega} \tag{1}$$

where the time delay T_d depends on the operator, the type of plant and the reference signal. According to the crossover model, this description of the open-loop transfer function holds true in a 1-1.5 decade frequency range centered at the crossover frequency [1]. What the human operator evidently does when acting as a controller in the pursuit tracking task is to choose (or achieve) a crossover frequency ω_c and time-delay T_d, then invert or compensate for the plant and joystick dynamics to produce an open-loop transfer function of an integrator with time delay (as in Eq. (1)).

Ample experimental evidence reveals that trained human operators can extract good tracking performance from various plants, yielding open-loop transfer functions in the form of Eq. (1). Values for ω_c and T_d have even been tabulated for various types of reference signal and various types of plant dynamics, including K, K/s, and K/s^2, where K is a gain [1]. In general, the more difficult the task, the lower the crossover frequency ω_c and the higher the time delay T_d. In our experiments, we shall adopt a simple plant dynamics: unity gain or $P = 1$. We shall also use ω_c as a performance metric.

III. Methods

Two distinct experiments were used in conjunction to construct and test our approach to biodynamic feedthrough cancellation. The first is aimed at constructing the model $\hat{H}$ of the biodynamic system, or determining parameter values for an auto-regressive moving average (ARMA) model, as described in section III-A. The second experiment tests the efficacy of the cancellation controller at improving tracking performance. In the second experiment, we pay particular attention to the design of the reference signal, to maximize the value of the data for characterizing tracking performance, as discussed in section III-B. Finally, subsection III-C presents the protocol used in the first and second experiments, describing the tasks undertaken by the human subjects.

A. Identification of the biodynamic system

Construction of the estimate $\hat{H}$ relies on data from a system identification test that takes place prior to implementation of the cancellation controller, but using the same hardware. The test involves the human subject and measurement of vehicle acceleration $\ddot{x}_v$ and the hand/joystick interaction force. A force sensor in the joystick can only measure the total force f, which is the sum of the biodynamic force f_b', the volitional force f_t, and the driving point impedance response f_{jb} of the operator (see Figure 3). However, if joystick motion is prevented, say, by a peg that locks it in a vertical position during the system identification test, then the impedance Z_{22} will not be excited and $f_{jb} = 0$. If further the subject is not given any task and is asked to not produce any force by volition, then f_t can be assumed to be small. Under these conditions, and assuming that the force and acceleration signals in question can be represented as linear functions of the Laplace variable s, then

$$H(s) = \frac{F_b'(s)}{s^2 X_v(s)} = \left.\frac{F(s)}{s^2 X_v(s)}\right|_{\dot{x}_j=0,\, f_t=0} \tag{2}$$

For the biodynamic model $\hat{H}$, we assumed an ARMA model structure in the form of a difference equation with constant parameters c_i, $(i = 0, 1, ..., 4)$ and d_j, $(j = 1, ..., 4)$

$$f_b'(n) = \sum_{i=0}^{4} c_i\, \ddot{x}_v(n-i) - \sum_{j=1}^{4} d_j\, f_b'(n-j), \tag{3}$$

where the signals f_b' and $\ddot{x}_v$ are represented in discrete time and n indexes discrete samples. To re-arrange the difference equation into a structure useful for fitting parameter values, we defined a data matrix A and a parameter vector $\underline{b}$ as

$$\begin{aligned} A &= [\underline{\ddot{x}}_v(n),\, \ldots,\, \underline{\ddot{x}}_v(n-4),\, -\underline{f}_b'(n-1,)\, \ldots,\, -\underline{f}_b'(n-4)] \\ \underline{b} &= [c_0,\, \ldots,\, c_4,\, d_1,\, \ldots,\, d_4]^T, \end{aligned} \tag{4}$$

where underbars on $\ddot{x}_v$ and f_b' indicate column vectors of discrete data that march back in time by row and arguments that indicate shifting of the entire column in discrete time. Thus the construction of matrix A facilitates the least-squares solution for the parameters contained in $\underline{b}$ using the pseudoinverse

$$\underline{b} = (A^T A)^{-1} A^T \underline{f}_b'(n) \tag{5}$$

The form of the model $\hat{H}$ in Eq. (3), in particular the fourth order and zero relative degree, were chosen based on observations of the experimental transfer function estimate constructed from experimental data of acceleration and force using the MATLAB function `tfe`.

Data were collected using white noise (bandpass filtered 0.7-4 Hz) to produce motion of the platform, whose acceleration $\ddot{x}_v$ was measured with an accelerometer, filtered with an analog anti-aliasing filter, and recorded. The maximum amplitude accelerations recorded were 0.75 g. A human subject sat in the platform chair with their hand grasping the joystick but not performing any task. The joystick's angular position was fixed relative to the platform with a snug-fitting steel peg inserted through its structure. A load cell in the stem of the joystick sensitive to shear forces measured the joystick force f_b', which in turn was anti-alias filtered and recorded. Although platform motion control was managed at 1000 Hz, data recording occurred at 100 Hz and the test lasted for 2 minutes. Before processing, the data were low-pass filtered (fifth order Butterworth filter, f_c=10Hz) and down-sampled to 50 Hz.

A typical experimental run for a representative human subject produced the transfer function estimate shown in Figure 4 as a swath of dots on the magnitude and phase versus frequency axes. Two peaks separated by a notch at about 6 Hz appear in the magnitude plot, supporting the choice of a fourth order model. Higher order models did not produce better fits. The continuous traces on the Bode plot in Figure 4 show the frequency response of the model fit to the same data. The model parameters were computed using Eq. (5) and

this model was excited with white noise to produce a simulated joystick force response that in turn was fed into the MATLAB `tfe` function.

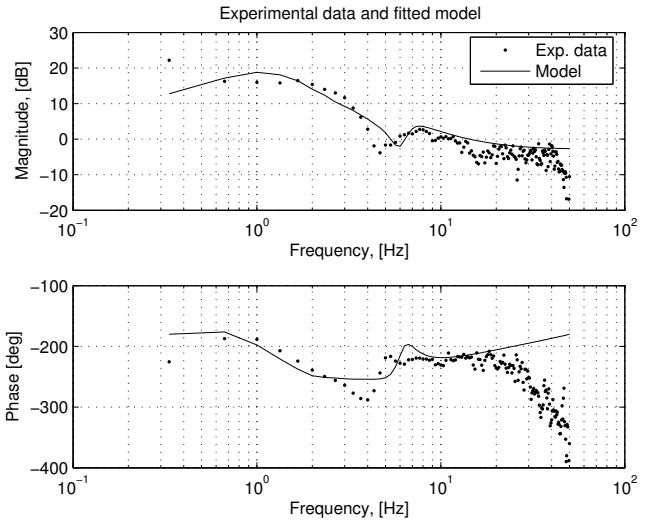

Fig. 4. The frequency response of the force f_b' to the excitation $\ddot{x}_v$ during the system identification test is shown for one subject. The Bode plot of the model $\hat{H}$ fit to the experimental data is shown in a continuous line.

B. System identification of volitional tracking

In contrast to the parametric form of the model used for system identification of the biomechanical subsystem, we used a non-parametric model for the tracking loop. We are interested in characterizing the tracking loop in the frequency domain, using the frequency response of the open-loop transfer function, as inspired by the crossover model.

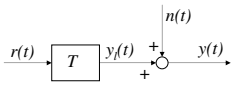

Fig. 5. A generic nonlinear system expressed as the sum of a *describing function* T and a remnant $n(t)$.

To introduce the design of a reference signal x_r that best facilitates identification of the open-loop tracking transfer function, let us consider the generic system shown in Figure 5. Let the transfer function G from $r(t)$ to $y(t)$ be expressed as the sum of a describing function T and a remnant or noise input $n(t)$. Since we assume that the signals $y_l(t)$ and $n(t)$ are not measurable, the challenge is to design $r(t)$ such that the best estimate $\hat{T}$ can be extracted from the signals $r(t)$ and $y(t)$.

Beginning with the cross-correlation function $\phi_{ry}(\tau)$, defined as

$$\phi_{ry}(\tau) = \lim_{\theta\to\infty} \frac{1}{2\theta} \cdot \int_{-\theta}^{\theta} r(t+\tau)y(t)dt, \tag{6}$$

and the autocorrelation function $\phi_{rr}(\tau)$ defined similarly, one may divide the cross-correlation spectral density (CSD) $\Phi_{ry}(j\omega)$ by the power spectral density (PSD) $\Phi_{rr}(j\omega)$ to obtain an estimate $\hat{G}$ for the transfer function $g(j\omega)$, where $\Phi_{ry}(j\omega)$ and $\Phi_{rr}(j\omega)$ are the Fourier transforms of $\phi_{ry}(\tau)$ and $\phi_{rr}(\tau)$, respectively.

Because the Fourier transform and cross-correlation are linear operators, one may write:

$$\begin{aligned} \hat{G}(j\omega) &= \frac{\Phi_{ry}(j\omega)}{\Phi_{rr}(j\omega)} = \frac{\Phi_{r(y_l+n)}(j\omega)}{\Phi_{rr}(j\omega)} = T(j\omega) + \frac{\Phi_{rn}(j\omega)}{\Phi_{rr}(j\omega)} \\ &= T(j\omega) + \frac{\int_{-\infty}^{\infty} e^{-j\omega\tau}\cdot\phi_{rn}(\tau)d\tau}{\Phi_{rr}(j\omega)} \end{aligned} \tag{7}$$

which expresses the estimate $\hat{G}$ as the sum of a describing function $T(j\omega)$ and a remnant or error term. The error term can be made small if $r(t)$ and $n(t)$ are uncorrelated by using a maximally long test time. Alternatively, the error term may be minimized by increasing its denominator, or increasing the value of the PSD of the reference signal for the frequency range of interest. Since the expression in Eq. (7) holds at any frequency $\omega = \omega_k$, an estimate $\hat{G}(j\omega_k)$ closest to $T(j\omega_k)$ at that frequency can be obtained by exciting the system with $r(t) = L\sin(\omega_k)$, where L is a limit set to avoid saturations in the signals $r(t)$ or $y(t)$. This observation suggests a test paradigm in which the frequency response $\hat{T}$ is reconstructed from a set of estimates, each taken at a particular frequency ω_k, chosen to span the frequency range of interest. If it is further supposed that T is linear and time invariant (LTI), then superposition holds and the resulting estimate is not dependent on the particular amplitudes or frequencies chosen in $r(t)$. Furthermore, estimates can be constructed simultaneously using a sum of sinusoids for the input signal $r(t)$. The magnitude and phase estimates are available only at each frequency ω_k, and appear as isolated dots on a Bode plot. The estimate $\hat{T}$ is then constructed by fitting or interpolating among these dots.

This approach has been used in previous work on pursuit tracking. It is common practice, in fact, to report the frequency response of pursuit tracking using isolated points on a Bode plot [15], [2], [5], [16] and [17].

In the present work, a sum of fifteen sinusoids was used for the reference signal $x_r(t)$. Even though this signal is periodic, it is random appearing due to its complexity and therefore eliminates precognitive tracking. Special attention was paid to the choice of frequencies and their amplitude, following the recommendations in [18]. To ensure that the reference signal had zero mean over the 180 second test time, the period of each sinusoid was chosen to be an integer ratio of 180. The frequencies of the component sinusoids were chosen to be relative prime multiples of the fundamental frequency 0.0055 Hz. The frequencies of the fifteen sinusoids were distributed evenly (on a logarithmic frequency scale) in the range between 0.01 Hz and 4 Hz, using the prime multipliers 2, 3, 5, 7, 11, 17, 23, 37, 59, 87, 131, 199, 310, 467, and 719.

The amplitudes of the 15 sinusoids were enveloped with an exponential function of frequency as follows:

$$x_r = 0.75\sum_{k=1}^{15} e^{-0.14(k-1)}\sin(\omega_k t + \phi_k) \tag{8}$$

The decay rate -0.14 and the scaling factor 0.75 were determined experimentally so as to keep the target inside the screen

but utilize much of the available space. Also, attention was paid to make sure the signal would contain sufficient energy at high frequencies to impose a suitable tracking challenge. The phase angles ϕ_k of the sinusoids were randomized before each test to eliminate any use of memory by the subjects. Code was written in MATLAB to numerically compute the open-loop tracking transfer function estimate for the fifteen angular frequencies.

C. Human subject test protocol

Human subject tests were used to experimentally verify the proposed solution. The subjects carried out a pursuit tracking task with a motion stick in the motion platform under three conditions. First, to establish individual baseline tracking performance, each subject used the joystick to track a target while the platform remained stationary. Second, to demonstrate tracking performance degradation due to ride motion, the subject used the joystick to track a target while the platform moved under white noise input and without cancellation torque on the joystick. In tests under the third and final condition, the subject used the joystick to track a target while the platform moved under white noise input and while the cancellation controller imposed torque on the motorized joystick. Tests under this third condition were used to determine the extent to which the controller restores tracking performance in a moving environment.

Twelve subjects were tested, ten men and two women aged 22-31. The subject pool did not include the authors. Each subject provided informed consent according to University of Michigan human subject protection policies. Each subject had several hours of past experience with the apparatus using the joystick for tracking with and without the platform moving. Each subject was given at least three minutes of additional practice time before each test and the order of the three tests was randomized to reduce the effects of learning and fatigue. The subjects were not told when the compensator was on or off. Each subject was buckled up in a seat attached to the platform using a four-point harness. Each subject grasped the single-axis joystick with his or her right hand and were instructed not to use the elbow rest.

Our experimental apparatus, shown in Figure 6, features a 2.24 kW brushless DC servo motor (Koll Morgan Goldline B 404-B-A3) that moves the platform on linear guides by means of a ball screw. The platform moves only in the lateral direction, and has a ± 0.15 m workspace. A high-resolution resolver is integrated into the motor housing and the motor moves under the control of a position feedback loop closed within the motor amplifier. This position follower is commanded with filtered white noise generated by a PC and transmitted through an interface card by ServoToGo Corp. The platform bandwidth was confirmed to exceed 10Hz. The accelerometer used to measure platform motion is located on the body of the joystick, which is rigidly mounted to the platform. Special care was taken in the design of the platform and chair to minimize structural dynamics between the chair seat and joystick mount.

The joystick has an angular workspace of $\pm 30^\circ$ and features encoder output with a resolution of 4096 counts per revolution.

Fig. 6. The single-axis motion platform is driven by DC motor and ballscrew and features a joystick accessible to the right hand of a seated operator.

The joystick is coupled to a 150W DC servo motor (Maxon RE 040) through a capstan drive. The torque applied by the DC motor on the joystick is computed as the product of the force necessary to apply in the center of the joystick grip and the distance from the joystick pivot to the center of the grip (0.08m).

A 15 inch computer monitor was positioned on fixed ground about 1.5 m in front of the subject. White lines 1 mm thick on a black background were used to draw a square target box of 30 mm width that moved horizontally on the lower part of the screen according to the signal $x_r(t)$. White lines were also used to draw a cursor in the form of a cross that moved under the control of the plant output $x_p(t)$. The vertical position of the joystick placed the cursor in the center of the screen. One radian of joystick angular displacement x_j was displayed as 0.6 m of displacement on the screen.

1) Performance Metrics: To quantify the success of tracking under the various experimental conditions, three performance metrics were defined. The first metric is the root-mean square average tracking error, denoted RMS. The second, called Dwell Ratio and denoted r_d, was defined as the ratio of time the cursor lay inside the square target relative to the total test time. This *time-on-target* definition is based on the notion that in many applications the target can be hit even if the aiming device does not point exactly at the center. The third is the crossover frequency f_c in Hz, defined as the frequency at which a line of -20 dB/decade slope fit to the magnitude frequency response estimate crossed the 0dB axis. After the fifteen dots were obtained on a frequency domain plot using Equation 7, a straight line with a slope constrained to -20 dB/decade was fit to the first eleven points using the method of least squares. The lowest eleven frequencies range up to 1 Hz, which is the typical upper limit of human tracking performance. A small RMS error, a large Dwell Ratio and a large crossover frequency are indicative of good tracking performance.

In addition to using single numbers that characterize an entire three minute tracking task for each human subject, we

also defined two moving averages. The first such average was defined for the Dwell Ratio using an indicator function that returns one whenever the cursor is inside the target box, and zero otherwise, then averaging this function over a running 10 second window throughout the test. The mean and standard deviation of the results obtained for the twelve subjects were computed and plotted against time for each test condition. The second moving average was defined for RMS error, also computed as the average over a running ten second time window.

IV. Results

After fitting an individualized biodynamic model to the characterization data taken with the pegged joystick, the tracking performance of each subject was tested under the three conditions: (A) baseline (stationary platform), (B) motion disturbance uncompensated and (C) motion disturbance compensated. Results indicate that motion disturbance has a significant deleterious effect on tracking performance and that compensation significantly reduces that effect. Performance was significantly improved with the compensating controller, but not quite restored to baseline levels. Since the compensating controller used for each subject was based on a biodynamic model individualized to that subject, we first present and compare the 12 biodynamic model fits. We then review the performance differences between the three conditions using our various performance metrics, including RMS error, Dwell Ratio, and crossover frequency.

A. Biodynamic model fits

Using the least squares fit to the $\ddot{x}_v$ and f_b' data, a biodynamic model was constructed for each of the 12 subjects. Values for the 9 parameters in the difference equation model locate four zeros and four poles in the discrete z-plane or equivalently, certain notches and peaks in the frequency domain. Although the fit was performed using time-domain techniques, here we present and compare the frequency responses of the 12 biodynamic models in Figure 7. Each biodynamic model fit features a notch in magnitude between 5 and 8 Hz followed by a small peak. Because a model form with zero relative degree was chosen, the magnitude flattens and phase returns to 180° at high frequencies. The nominal 180° phase difference between $\ddot{x}_v$ and f_b' is appropriate to our sign convention for x_v and f_b'. If one uses 10dB to approximate the magnitude at low frequencies in Figure 7, then the DC gain of the biodynamic force f_b' is moderately small at 3.2 N per 1 m/s^2 acceleration or 32 N per g of acceleration. We are most interested in the features that appear in the 0.1-10 Hz range, since this is the frequency range that characterizes human tracking performance and biodynamic feedthrough.

Note that the biodynamic model can be expected to be a function of the subject's body posture, the restraints used, the configuration of the joystick axis, the joystick length, and the degree of muscle co-contraction adopted by the subject, and tightness of grip. The biodynamic model also reflects such effects as the stretch reflex and possibly other reflex loops, but hopefully does not reflect any effects of volitional control

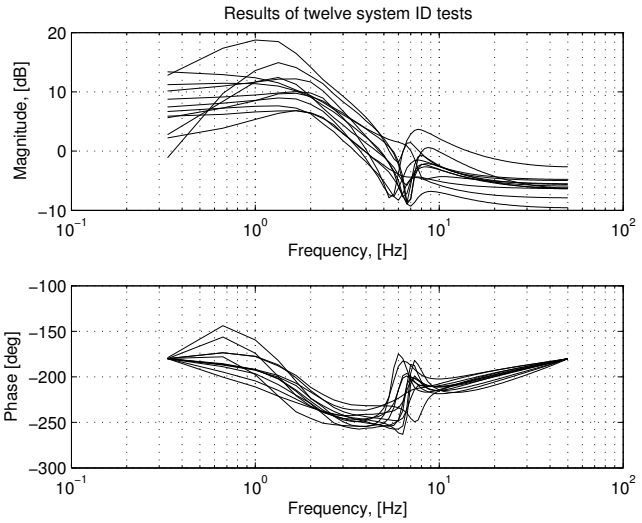

Fig. 7. System identification results for twelve subjects. The models show similar trends, but it appears that hey cannot be substituted with a single, average model. We therefore propose the construction of a separate controller for each individual.

(something that certainly depends on conformance by each subject to experiment instructions).

B. Tracking Performance Results

Before presenting summary results and statistics across the 12 subjects and across the 180 second trial time, let us first present some time trajectories. Figure 7 shows trajectories of the reference $x_r(t)$ and plant output $x_p(t)$ for one subject during a typical 20-second period of the 180 second trial. In separate plots, tracking performance is shown for each of the three conditions (A) stationary platform, (B) moving platform uncompensated and (C) moving platform compensated. In each of the three plots, the solid line is the reference signal x_r and the dashed line is the plant output x_p. It can be seen in (A) that the operator produces an output x_p that is a delayed and low-pass filtered version of x_r. In plots (B) the tracking performance is noticeably deteriorated by the presence of platform motion feeding through the biodynamic subsystem. In (C) the compensator has restored tracking performance almost back to the level of the stationary platform case (A).

For each condition, the tracking error or difference between the x_r and x_p signals was used to compute an average error across the 12 subjects. These average errors are further processed using RMS computed over a moving 10 second window and presented as the thick black line in Figure 8. Gray shading extends one standard deviation above and below the RMS trace. Comparing plots for the conditions (A), (B), and (C) in Figure 8 reveals that platform motion degrades performance and increases variance across the 12 subjects and that compensation partially restores that performance but does not significantly decrease the variance across the 12 subjects.

Figure 9 shows similar moving averages of the Dwell Ratio for the 12 subjects. The traces in Figure 9 indicate the fraction of time that all 12 subjects located their cursors within target during a 10 second moving window, where higher values

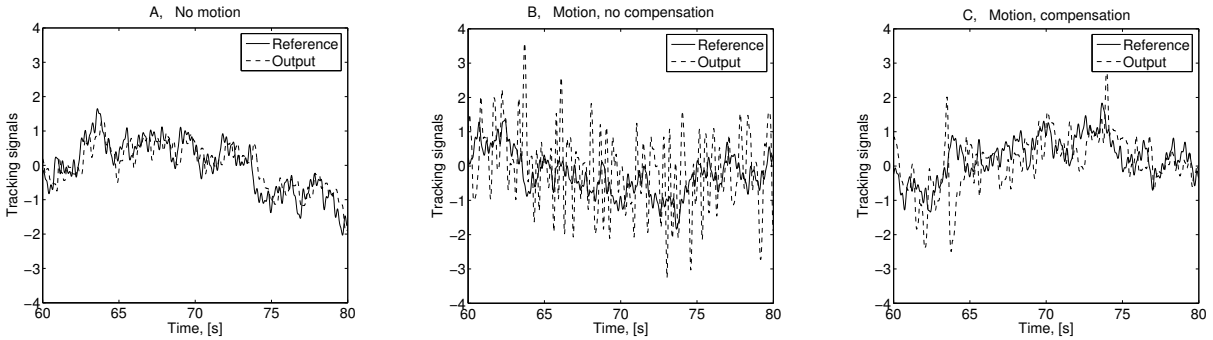

Fig. 8. Twenty seconds of the reference x_r and plant output x_p signals are shown for a typical subject under the three experimental conditions: (A) stationary platform (B) moving platform without compensation (C) moving platform with compensation.

indicate better performance. Figures 9 (A) and (B) show that platform motion degrades performance while Figure 9 (C) shows again that compensation partially restores performance.

Note that the traces in Figures 8 and 9 show data over the full 180 seconds of test-time per trial, from which trends across the 180 seconds might be inferred, trends such as learning, loss of attention, or fatigue. Performance seems steady for the most part, with the possible exception of condition (B), where a slight increase in RMS error and drop in Dwell Ratio over the 180-second trial is apparent. We did not, however, evaluate the significance of this trend.

Summary statistics were computed for the RMS error and Dwell Ratio by condition across the 12 subjects and collapsed over the 180 second trial period. The median RMS errors for the three conditions are presented as lines through the middle of boxes in the box-and-whisker plot in Figure 11. The boxes enclose the lower and upper quartiles and the whiskers show the range of the data. Similarly, the box-and-whisker plot in Figure 12 shows the summary statistics for the Dwell Ratio by condition across the 12 subjects and collapsed over the 180 second trail period. Differences in RMS error and Dwell Ratio by condition are clearly evident in Figures 11 and 12.

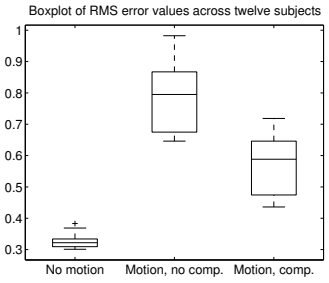

Fig. 11. Boxplot of RMS error values across the twelve subjects under the three test conditions

Using the methods outlined in Section III above, we extracted the magnitude and phase response at a set of 15 frequencies for a particular set of input sinusoid amplitudes. In accordance with the crossover model, we fit lines of -20 dB/decade slope to the series of magnitude response points, using only the first 11 points (those near the resulting crossover frequency). Figure 12 presents the frequency response of the transfer function that relates the output x_p to the error x_e

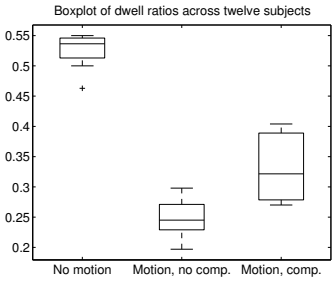

Fig. 12. Boxplot of Dwell Ratios across the twelve subjects under the three test conditions

TABLE I

PERFORMANCE METRICS BY CONDITION: A. STATIONARY, B. MOVING WITHOUT COMPENSATION, AND C. MOVING WITH COMPENSATION.

Metric	A. No motion	B. No comp.	Comp.
RMS error	4.04	9.62	7.01
r_d	0.48	0.23	0.31
$f_c, [Hz]$	0.25	0.10	0.14

for a representative subject, for each of the conditions. The estimates at each of the 15 frequencies are shown as dots in both the magnitude and phase plots. For each condition a line of -20 dB/decade slope was fit to the first 11 magnitude points, as shown. From those best-fit lines, the crossover frequencies were determined for each condition. In Figure 12 a crossover frequency of 0.4 Hz can be seen for the stationary platform case in (A), of 0.1 Hz for the moving, uncompensated case in (B) and of 0.25 Hz in the moving, compensated case in (C). This trend (lower crossover with a moving platform, but partial restoration with compensation) is typical of all 12 subjects.

Figure 14 presents a box-and-whisker plot of the crossover frequency values obtained for the twelve subjects under the three experimental conditions. The changes in crossover frequency demonstrate tracking performance degradation as a result of platform motion and a partially restored tracking performance as a result of compensation.

To analyze statistical significance of the differences by condition, multiple-factor analysis of variances (MANOVA) was applied to the three performance metrics (RMS error, Dwell Ratio, and crossover frequency), revealing significant main effects due to condition and subject, with no significant

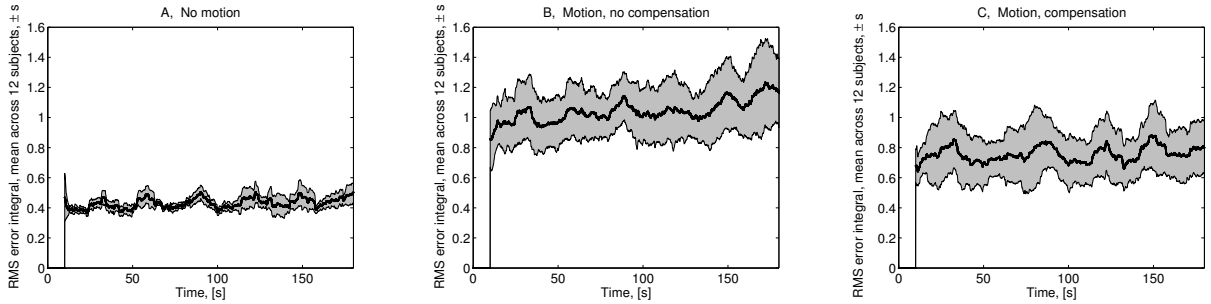

Fig. 9. RMS error averages with ten second moving time windows under the three test conditions

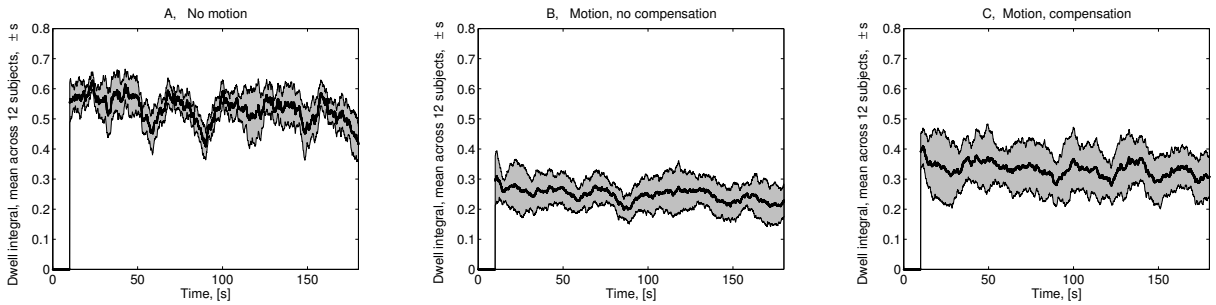

Fig. 10. Dwell ratios averages with ten second moving time windows under the three test conditions

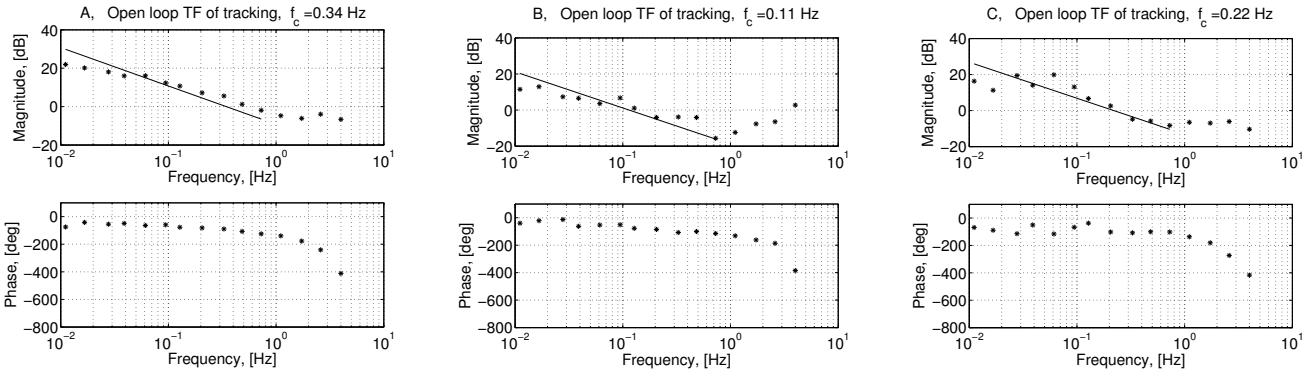

Fig. 13. Open loop transfer function of tracking under the three test conditions

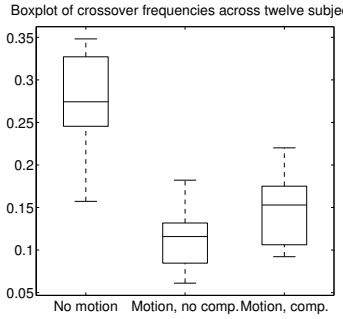

Fig. 14. Boxplot of crossover frequencies across the twelve subjects under the three test conditions

interaction effects. Thereafter, paired t-tests were applied to each of the performance metrics comparing conditions (A) and (B) and likewise conditions (B) and (C). These mean values for the performance metrics are presented in Table I. The differences between (A) and (B) as well as the differences between (B) and (C) were all significant, achieving p-values well below a threshold α level of $p = 0.01$, indicating significant degradation in tracking performance with the addition of platform motion and that the addition of the compensating controller significantly improves tracking performance according to all three performance metrics.

V. Discussion and Conclusions

Manual control is significantly more difficult onboard a moving vehicle than on solid ground. Vehicle motion affects human perception and human action in ways that are dependent on body configuration, on vibration frequency, and on the configuration of the axes of the manual control interface. We have shown how a model-based controller acting through a motorized joystick can be used to mitigate the effects of vehicle motion on manual control. We developed our model for biodynamic feedthrough based on a careful consideration of the operator's body as a two-port between the seat and the joystick handle. Even if the vehicle is assumed to act as a perfect motion source on the operator's body, two transfer

functions are still at play: a transmittance relating vehicle motion to joystick force and a driving-point impedance of the operator's body as seen by the joystick. These were both considered in the design of a system identification experiment aimed at producing a model suitable for cancellation of biodynamic feedthrough.

Results indicate that the cancellation controller performs quite well. Performance differences were also noticeable to the experimental subjects. In post-experiment interviews, the subjects indicated that they felt comfortable with the compensating controller, that they felt its action in the feel of the joystick but did not find it distracting, and that they trusted it to help improve their performance.

The objective of our future work is to compare the performance improvement offered by a motorized joystick to improvement available by other means, including changes to body configuration and degrees of freedom available in the manual interface, use of an armrest or other constraint, and use of a model-based filter rather than controller acting through a motor. We are also interested in using structures for the biodynamic feedthrough function that are based on multibody dynamic models of the human operator. We expect that such models might be more capable of extrapolation or of predicting the relative merits of various countermeasures. Future work will also include the development of adaptive cancellation controllers. Current work that will be reported in a subsequent paper is focused on the sister class of systems, in which biodynamic feedthrough closes a loop between the vehicle and joystick.

VI. Acknowledgments

The authors would like to express their gratitude to the test subjects who spent many hours on the platform. Also many thanks to our sponsor, the Automotive Research Center at the University of Michigan and to the RMS team at the Army-TACOM for their support. Thanks are also due to Dan Repperger of Wright Patterson Airforce Base for valuable consultations and the loan of the motion platform.

References

[1] T. B. Shridan and W. R. Ferrell, *Man-Machine Systems: Information, Control, and Decision Models of Human Performance*. The MIT Press, 1974.

[2] D. McRuer, "Human dynamics in man-machine systems," *Automatica*, vol. 16, pp. 237–253, 1980.

[3] R. W. McLeod and M. J. Griffin, "A review of the effects of translational whole-body vibration on continuous manual control performance," *Journal of Sound and Vibration*, vol. 133, no. 1, pp. 55–115, 1989.

[4] R. A. Hess, "Theory of roll-ratchet phenomenon in high-performance aircraft," *Journal of Guidance, Control and Dynamics*, vol. 21, no. 4, pp. 101–108, January-February 1998.

[5] R. A. Hess, "Analyzing manipulator and feel system effects in aircraft flight control," *IEEE Transactions on Systems, Man and Cybernetics*, vol. 20, no. 4, pp. 923–931, July/August 1990.

[6] F. Arai, J. Tateishi, and T. Fukuda, "Dynamical analysis and suppression of human hunting in the excavator design," *Proceedings of the 2000 IEEE International Workshop on Robot and Human Interactive Communication, Osaka, Japan*, September 27-29 2000.

[7] N. R. Parker, S. E. Salcudean, and P. D. Lawrence, "Application of force feedback to heavy duty hydraulic machines," in *Proceedings of the IEEE International Conference on Robotics and Automation*, vol. 1, pp. 375 – 381, May 1993.

[8] D. Repperger, A. Koivo, and M. Haas, "Using a hidden markov process to both characterize critical human tracking regions and to predict the incidence of pilot induced oscillation," in *Proceedings of the American Control Conference*, vol. 1, pp. 443 – 447, 4-6 June 1997.

[9] M. Verger, A. Grunwald, and S. Merhav, "Suppression of biodynamic disturbances and pilot-induced oscillations by adaptive filtering," *Journal of Guidance*, vol. 7, no. 4, pp. 401–409, July-August 1984.

[10] M. Verger, A. Grunwald, and S. Merhav, "Adaptive filtering of biodynamic stick feedthrough in manipulation tasks on board moving platforms," *Journal of Guidance*, vol. 11, no. 2, pp. 153–158, march-April 1988.

[11] R. B. Gillespie, C. Hasser, and P. Tang, "Cancellation of feedthrough dynamics using a force-reflecting joystick," *Proc. ASME Dynamic Systems and Controls Division*, pp. 319–326, 1999.

[12] S. Sövényi and R. Gillespie, "An investigation of vibration feedthrough and feedthrough cancellation in joystick controlled vehicles.," *2003 International Mechanical Engineering Congress and R and D Expo, IMECE2003-41598, Washington, D.C. USA, ASME Dynamic Systems and Control Division, DSC*, vol. 72, no. 1, pp. 567–576, 2003.

[13] M. R. Sirouspour and S. E. Salcudean, "Robust controller design for canceling biodynamic feedthrough," *8th International Symposium on Experimental Robotics, ISER*, July 8-11, 2002.

[14] M. Sirouspour and S. Salcudean, "Suppressing operator-induced oscillations in manual control systems with movable bases," *IEEE Transactions on Control Systems Technology*, vol. 11, no. 4, pp. 448–459, July 2003.

[15] D. T. McRuer, R. W. Allen, D. H. Weir, and R. H. Klein, "New results in driver steering control models," *Human Factors*, vol. 19, no. 4, pp. 381–397, 1977.

[16] R. Hess, "Theory for roll-ratchet phenomenon in high performance aircraft," *Journal of Guidance, Control and Dynamics*, vol. 21, no. 1, pp. 101–108, Jan-Feb. 1998.

[17] D. Johnston and B. Aponso, "Design considerations of manipulator and feel system characteristics in roll ratcheting," *NASA CR-4111*, Feb. 1988.

[18] D. W. Repperger, D. B. Rogers, J. W. Frazier, and K. E. Hudson, "A task difficulty - G stress experiment," *Ergonomics*, vol. 27, no. 2, pp. 161–176, 1984.